Scalings of energetic particle transport by ion temperature gradient microturbulence[a)]

Wenlu Zhang,[1,2,b)] Viktor Decyk,[3] Ihor Holod,[1] Yong Xiao,[1] Zhihong Lin,[1] and Liu Chen[1,4]
[1]*Department of Physics and Astronomy, University of California, Irvine, California 92697, USA*
[2]*CAS Key Laboratory of Basic Plasma Physics, University of Science and Technology of China, Hefei, Anhui 230026, China*
[3]*Department of Physics and Astronomy, University of California, Los Angeles, California 90095, USA*
[4]*Institute for Fusion Theory and Simulation, Zhejiang University, HangZhou, Zhejiang 310058, China*

(Received 16 November 2009; accepted 12 March 2010; published online 7 May 2010)

Transport scaling of energetic particles by ion temperature gradient microturbulence in magnetized plasmas is studied in massively paralleled gyrokinetic particle-in-cell simulations. It is found that the diffusivity decreases drastically at high particles energy (E) to plasma temperature (T) ratio because of the averaging effects of the large gyroradius and drift-orbit width, and the fast wave-particle decorrelation. At high energy, the diffusivity follows a $(E/T)^{-1}$ scaling for purely passing particles, a $(E/T)^{-2}$ scaling for deeply trapped particles and a $(E/T)^{-1}$ scaling for particles with an isotropic velocity distribution since the diffusivity therein is contributed mostly by the passing particles. © *2010 American Institute of Physics*. [doi:10.1063/1.3379471]

I. INTRODUCTION

Energetic particles can be created in magnetically confined plasmas through fusion reactions (α-particles) and auxiliary heating such as neutral beam injection (NBI) or radio frequency heating (RF). Generally, α-particle distribution is isotropic in velocity space, while the NBI mainly contributes passing populations and a large portion of RF heated particles are deeply trapped particles. These energetic particles are subject to the interaction with magnetohydrodynamic (MHD) instabilities,[1] microturbulence,[2] stochastic magnetic field,[3] and classical collisional and orbital effects.[4] The interaction between energetic particle and background field could be twofold: they may drive a new type of instabilities, for example, Alfvén eigenmodes, energetic particle modes, etc. On the other hand, the microturbulence could affect the confinement of the energetic particles. The confinement of the energetic particles is of great importance in burning plasma, for example, the International Thermonuclear Experimental Reactor (ITER),[5] since the ignition relies on the self-heating by the energetic fusion products and the escaped energetic particles can pose a significant heat load to the plasma facing materials. The diffusion of the energetic particles such as the cosmic rays by microscopic turbulence is also an important scientific issue in the space and astrophysical plasmas.[6]

Based on the earlier theoretical studies[7] and simulations,[8] the conventional concept suggests that in burning plasmas, energetic-particle transport by microturbulence is reduced by orbit averaging and wave-particle decorrelation. Therefore, energetic particle confinement is much *better* than thermal ion confinement in the absence of long-wavelength MHD instabilities. Both orbit averaging and wave-particle decorrelation effects depend on the relevant spatial and temporal scales, which are determined by the ratio of particle energy E to plasma temperature T. Experimental database[4,9] in the large energy regime ($E/T>10$) confirmed this theory prediction by showing that the upper limit to the diffusivity of energetic particles is one order of magnitude smaller than that of thermal ions. In recent publications[10–12] the energetic-particle transport of a slowing down distribution is found negligible in high energy regime.

However, recent fusion experiments[13,14] reported discrepancy between the measured and predicted distributions of NBI driven currents in the absence of MHD instabilities. Background microturbulence is believed responsible for the re-distribution of energetic ions through anomalous transport. Recent DIII-D NBI transport experiments[15,16] delivered the first evidence by measuring cross-field diffusion of energetic-particles by microturbulence that dominated by ion temperature gradient (ITG) instability. Discrepancy between experiment and classical collisional predictions is found to be more pronounced at low energy-to-temperature ratio (E/T), where strong microturbulence is expected. Inspired by this correlation, they found the expected transport by microturbulence is the right order of magnitude. Some recent theoretical[17] and computational[12,18] studies also suggested a significant transport level of the energetic particles driven by the microturbulence.

In order to resolve this discrepancy and clarify the uncertainty in the transport of energetic particles by microturbulence, here we study the diffusion of the energetic particles by the microscopic ITG[2] turbulence in large scale first-principles simulations of fusion plasmas using the global gyrokinetic toroidal code (GTC).[19] The ion radial spread as a function of energy and pitch angle is measured in the steady state ITG turbulence. Besides the radial spread increasing linearly with time, the probability density function (PDF) of the radial excursion is found to be very close to a Gaussian, indicating a diffusive transport from a random walk process.[10,20,21] The radial diffusivity as a function of the en-

[a)]Paper XI3 3, Bull. Am. Phys. Soc. **54**, 344 (2009).
[b)]Invited speaker. Electronic mail: wenluz@uci.edu.

ergy and pitch angle can thus be accurately calculated using the random walk model. We find that the diffusivity decreases drastically for high energy particles due to the averaging effects of the large gyroradius and drift-orbit width, and the fast decorrelation of the energetic particles with the ITG oscillations. By performing the integration in phase space, we can calculate the diffusivity for any distribution function. At high energy regime, the energetic-particle transport scales as $(E/T)^{-1}$ for purely passing particles due to the orbit averaging and fast decorrelation of parallel resonance, $(E/T)^{-2}$ for trapped particles due to gyroaveraging, banana orbit averaging and wave-particle decorrelation of drift-bounce resonance, and $(E/T)^{-1}$ for particle with isotropic velocity distribution since passing particles dominate transport in this energy regime. This result not only reconciles the differences between the older experiments[4] with a higher born energy and the newer experiment[13,14] with a lower born energy (relative to the plasma temperature), but also explains many features of recent DIII-D experiments.[15,16]

A. Orbit averaging

Canonical perturbation theory for a periodic Hamiltonian system[22–24] shows that orbit averaging follows strictly from the existence of a time-scale separation between equilibrium and perturbed motion. The orbit-averaged theory has been well established and widely applied in plasma physics.[7,10,25–39] However, in a recent letter,[40] the authors present a heuristic argument and simulation results, contradicting to the existing literatures,[7,10,25–30] that the concept of orbit averaging is invalid for the calculation of turbulent transport of energetic particles in a tokamak plasma if the particle orbit size (Δr) is larger than the turbulence eddy size (λ_c). This claim is of both fundamental and practical significance. Fundamentally, since the orbit-averaging effect is a necessary result of the orbit-averaged theory, the claim implies that the orbit-averaged theory is only valid if $\lambda_c > \Delta r$ [Eqs. 3 and 4 of Ref. 40]. The requirement of the spatial-scale separation contradicts the textbook notion[22–24] that only the time-scale separation is required for the validity of the orbit-averaged theory.[7,10,25–39] Practically, the requirement of the spatial-scale separation leads to an energy scaling in Ref. 40 different from that of the orbit-averaged theory[10,30] for the turbulent transport of energetic trapped particles in a burning plasma such as ITER.

From the point of view of the canonical perturbation theory,[22–24] the guiding center drift orbit-averaged theory is identical conceptually and mathematically to the gyroaveraged theory. Requiring $\lambda_c > \Delta r$ for the orbit-averaged theory is equivalent to requiring $\lambda_c > \rho$ for the gyrokinetic theory (ρ is the gyroradius), which clearly contradicts the gyrokinetic theory.[35–39]

We clarify that the orbit-averaged theory is valid for the turbulent transport of energetic particles in tokamak and demonstrate that the energy scaling of the turbulent transport predicted by the orbit-averaged theory is consistent with results from large scale gyrokinetic particle simulations. Therefore, the heuristic claim on the spatial-scale separation for the orbit averaging and the associated energy scaling of trapped particle transport in Ref. 40 are erroneous. We observe that the central claim in the letter of Ref. 40 has been published previously by the same authors as a regular article of Ref. 41 and later in Refs. 42 and 43 together with simulation results from gyrokinetic continuum flux-tube GENE code[40] supporting the erroneous energy scaling. Considering the fact that the claim of a spatial-scale separation for the orbit averaging contradicts the canonical perturbation theory, the gene simulation results in Refs. 40–43, consistent with the erroneous energy scaling are thus questionable.

II. SIMULATION APPROACH

A. Fully self-consistent ITG turbulence simulations

The energetic-particle transport by the ITG turbulence in burning plasma is investigated using GTC with multispecies capability. A global field-aligned unstructured mesh[20] is utilized in GTC to provide the maximal computational efficiency without any approximation in physics or geometry to describe nonlocal geometric effects and the toroidal eigenmodes with anisotropic structures. The tokamak with concentric flux-surface is described by magnetic coordinates (r, θ, ζ), where r is the radial coordinate labeling the flux surfaces, θ is the poloidal angle and ζ is the toroidal angle, respectively. Representative parameters of DIII-D tokamak H-mode core plasmas[44] has been used in the simulation, which have a peak ITG at a radial position $r=0.5a$ with the following local parameters: $R_0/L_T=6.9$, $R_0/L_n=2.2$, $q=1.4$, $\hat{s} \equiv (r/q)(dq/dr)=0.78$, $T_e/T_i=1$, $\epsilon \equiv a/R_0=0.36$, and $a/\rho_i=500$. Here R_0 is the major radius, a is the minor radius, $L_T \equiv [d \ln T/dr]^{-1}$ and $L_n \equiv [d \ln n/dr]^{-1}$ are the temperature and density gradient scale lengths, T_i and T_e are the ion and electron temperatures, q is the safety factor, $\hat{s}$ is the magnetic shear, ϵ is the inverse large aspect ratio, $\rho_i=v_i/\Omega_i$ is the gyroradius of thermal ions, v_i is the thermal velocity, and $\Omega_i=eB/m_ic$ is the gyrofrequency. These parameters give rise to a strong ITG instability. Our global simulations uses simplified physics models including a parabolic profile of $q=0.854+2.184(r/a)^2$, a temperature gradient profile of $\exp\{-[(r-0.5a)/0.28a]^6\}$, a circular cross section, electrostatic fluctuations with an adiabatic electron response, fixed boundary conditions with electrostatic potential $\delta\phi=0$ enforced at $r<0.1a$ and $r>0.9a$, no externally driven plasma flows or collisions,[45] and an effective collision operator modeling a heat bath[21] to prevent the relaxation of the temperature profile. The computational mesh consists of 32 parallel grids, and a set of 384×3072 unstructured radial and poloidal grids with a perpendicular grid size of ρ_i. These simulations evolved 4×10^8 thermal particles (gyrocenters) for 5000 time steps along with their interactions with the self-consistent electrostatic potential represented on the 4×10^7 spatial grid points. The default time step is $0.1L_T/v_i$.

The marker temperature and density are set up uniformly in these simulations, where very small random fluctuations are launched upon start and grows exponentially due to the ITG instability as evidenced in the early time history of the ion heat conductivity shown in the lower panel of Fig. 2. Zonal flows are then generated through modulational instability,[46,47] saturate the ITG instabilities after the time of

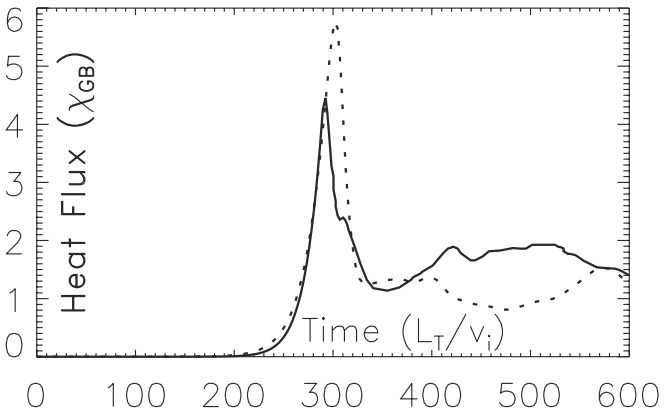

FIG. 1. The time history of heat flux between GTC (Ref. 19) (solid) and XGC (Refs. 51 and 52) (dotted) for $a/\rho_i=250$ and without heat source.

$t\approx 250L_T/v_i$ through random shearing of the zonal flows.[48] Finally, the nonlinear coupling of ITG-zonal flows leads to a fully developed turbulence after $t\approx 400L_T/v_i$ with a steady state transport level, which is insensitive to the initial conditions and is characterized by an averaged ion heat conductivity of $\chi_i=3.1\chi_{GB}$ over $t=[400,1000]L_T/v_i$. The gyro-Bohm unit for the heat conductivity of the thermal ions are defined as $\chi_{GB}=\rho^*\chi_B$, where $\rho^*=\rho_i/a$ and $\chi_B=cT_e/(eB)$. Here c and e are the speed of light and electron charge, respectively, and B is the on-axis magnitude of the magnetic field. The fluctuations in the steady state are nearly isotropic in radial and poloidal directions[21] with the perpendicular spectrum peaks around $k_\perp\rho_i=0.2$. GTC simulations of these ITG turbulence with similar parameters studying the energetic-particle transport by microturbulence,[10] the transport scaling with respect to the device size[20] and the turbulence spreading[21] that underlies the transition of the scaling have previously been carried out with extensive numerical convergences and cross-code benchmarks.[49] In particular, convergence with respect to the number of particles has been carefully studied to ensure that the particle noise does not affect the physics being studied. We found that the noise-driven flux[50] is consistently smaller than the ITG-driven flux by at least an order of magnitude when using 20 particles per cell, as shown in the lower panel of Fig. 2. Furthermore, Fig. 1 shows the benchmark between GTC (Ref. 19) and X-point included Guiding Center Code (XGC),[51,52] where a similar linear growth rate and steady-state turbulence level is displayed for the case of $a/\rho_i=250$ and without heat source.

B. Multispecies simulation capability

The GTC code has grown over the years from a single-developer code designed for a specific problem, to a prominent code with many users and contributors in the magnetic fusion energy community. It became imperative to reengineer (refactor) the code to allow multiple authors to contribute independently and to extend its capabilities to support new physics, such as the simulation discussed in this paper. This was done by applying object-oriented design principles to the FORTRAN90 code. Although FORTRAN90 is an object-based language that does not support inheritance, it does

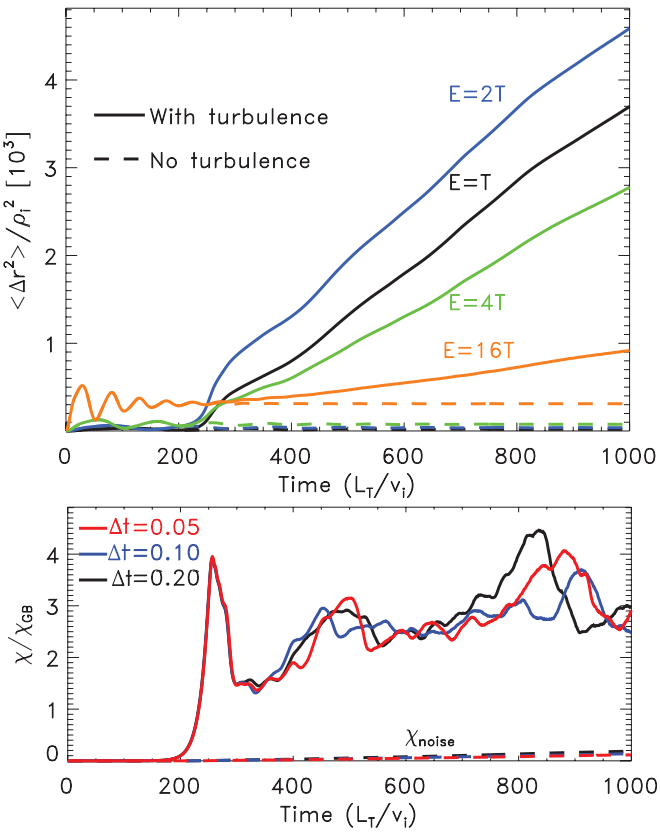

FIG. 2. (Color) Lower panel: Time history of thermal ion heat conductivity χ_i driven by ITG turbulence (solid) or by particle noise (dashed), measured in different runs with time step $\Delta t=0.2L_T/v_i$ (black), $\Delta t=0.1L_T/v_i$ (blue), and $\Delta t=0.05L_T/v_i$ (red). Upper panel: Time history of radial excursion $\langle\Delta r^2\rangle$ for particle energy $E/T_e=1$ (black), 2 (blue), 4 (green), and 16 (orange) when ITG turbulence is present (solid) or absent (dashed), where the time step is $\Delta t=0.1L_T/v_i$.

support object composition very well, and polymorphism can be implemented manually.[53]

In object-oriented design, user defined types are created which provide a kind of basis set for structuring the code data. Each type should represent the important concepts (abstractions) used in the code. The data inside the type is normally kept secret (encapsulated) and changeable, while the public usage (interface) of the procedures using the type is kept simple and stable. A class in FORTRAN90 consists of a module that contains a derived type definition and the procedures which use that type, plus any static data shared by the class. An object is a variable of the derived type, and a constructor is a procedure which assigns an initial value to an object. Generally, data cannot be modified outside this class except by calling procedures provided by the author of this class. As a result, an author of a class can make changes to its inner structure without interfering with other classes and authors.

In order that the code could be used for production while the changes were made, we proceeded in stages. Initially, an upper layer of classes was implemented which called the original GTC code under the hood. The derived types pointed at existing data in GTC, and the procedures called the original GTC subroutines. The original GTC code was modified only slightly. This allowed us to define and refine a

set of classes which described the important features of the GTC code in a new, more abstract way, with a minimum of implementation. The classes could be added one at a time, and at the end of each day, the code continued to work correctly. Ten classes were ultimately defined and implemented: gyrokinetic and drift kinetic particles, scalar and vector fields, a mesh, Jacobian, finite Lamor radius (FLR), equilibrium, interpolation, and particle descriptors. These classes provided a stable interface to future modifications.

In the second stage of this development, some of the scaffolding was removed. The constructors in the class objects now allocate the data and the array data in the original GTC code was removed. This isolates the components and allows multiple instantiations of the objects to be created, such as the multiple ion species used in the simulation discussed here. Again, the work was done incrementally, one class at a time, so that the code was always working properly.

The third stage of the work, still ongoing, was to integrate the capabilities of the various versions of the GTC code into one flexible and extensible version. To do this, we developed a methodology to implement design patterns in FORTRAN90.[54] Design patterns are abstract solutions to generic programming problems, which allow one to handle increased complexity. As an example, the strategy pattern was used in GTC to support multiple solvers.

III. SCALINGS OF ENERGETIC PARTICLE TRANSPORT

A. Statistics of radial diffusion and transport

In order to study the transport of energetic particles by the ITG turbulence, we measure the radial diffusion of the ions, with special interest to the high energy tails of the distribution function. For this purpose, we calculated the radial excursion of groups of trace particles in the phase space, specifically, a mesh of 23 grids in the kinetic energy $E=mv^2/2$ (up to $256T$) and 160 uniform grids in the pitch $\xi=v_\parallel/v$ for isotropic distribution in velocity space, where $v_\parallel$ is the local parallel velocity. For each velocity grid point, we initiate up to $N=2\times10^6$ particles uniformly distributed in a thin annulus domain of $r/a=[0.45,0.55]$, where the intensity of the turbulence is roughly flat, as evident in the lower panel of Fig. 3. We calculate the mean-squared radial displacement of each group of the particles

$$\langle \Delta r^2 \rangle = N^{-1}\sum_{i=1}^{N}[r_i(t_1)-r_i(t_0)]^2,$$

where $r_i(t_0)$ and $r_i(t_1)$ are the radial position of the ith particle at the beginning and the end of a time period $[t_0,t_1]$, respectively. As an example, the time history of the radial spreads for several energy groups (averaged over the pitch) are shown as the solid lines in the upper panel of Fig. 2. In order to compare the effects of turbulence scattering with equilibrium orbit width effects, the radial spreads of the same ions are also calculated in another identical simulation but with the ITG turbulence suppressed. The excursions due to the equilibrium orbits are presented as dashed lines in the same figure. The equilibrium spreads approach quickly to fixed amplitudes that are proportional to the energy as expected. This relaxation takes several bounce times $\tau=2\pi qR/(\sqrt{\epsilon}v)$, which is inversely proportional to the square root of energy, as clearly shown in Fig. 2. In the linear regime ($t<200L_T/v_i$), the turbulence is so weak that the equilibrium excursions (dashed lines) are identical to the perturbed excursions (solid lines) for all energy groups. After the turbulence reaches the steady state ($t>400L_T/v_i$) in the nonlinear regime, the difference between the equilibrium and perturbed excursions is relatively small for high energy ions (e.g., $E/T=16$), indicating that the turbulence exerts little influence on the high energy orbits. On the other hand, for a lower energy (e.g., $E/T=2$), the perturbed excursions is much larger than the equilibrium excursions, suggesting that the effect of the turbulence scattering dominates the radial excursions. To isolate the effects of the turbulence scattering from the equilibrium orbit width, turbulent excursions are subtracted by the corresponding equilibrium excursions to result in a net turbulence radial excursions, which increase linearly with time for all energy groups in the presence of the steady state ITG turbulence. This important feature is a strong evidence for a diffusive transport associated with the radial excursion of the ions by the turbulence scattering.

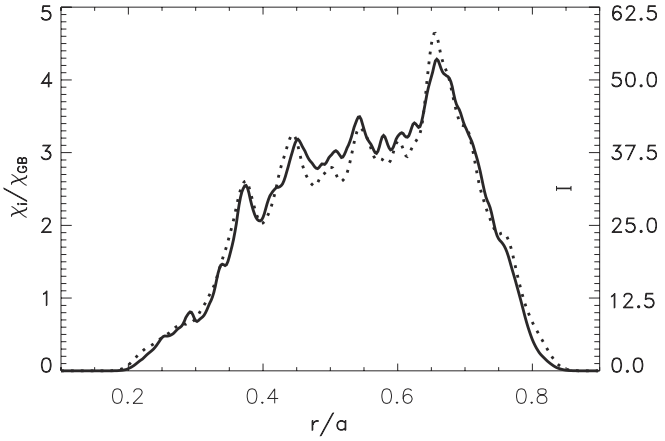

FIG. 3. Radial profiles of thermal ion heat conductivity χ_i and ITG intensity of fluctuating potential $I=(e\delta\phi/\rho^*T)^2$, where $\rho^*=\rho_i/a$.

The diffusive transport nature of the ITG turbulence is further supported by the fact that the radial profile of the heat conductivity matches very well with the intensity profile of the fluctuation potential, as shown in Fig. 3, which means that the transport is driven by the local fluctuation intensity.[21] Furthermore, the PDF of the electrostatic potential intensity of the ion heat fluxes and of the radial excursions[10] all decay exponentially with no significant tails. All the above features support the conclusion that the heat flux is carried by the radial diffusion of particles, and that large transport events, where heat pulses propagate ballistically, are apparently absent over this simulation time. Fundamentally, the stochastic wave-particle decorrelation[10,55–57] due to the overlaps of the phase space islands gives rise to the diffusive transport process. That is, the wave does not trap or convect the particles, but only scatters the particle orbits.

Since a Gaussian or Markovian dynamics describing the

microscopic random walk or Brownian motion is a necessary requirement for a diffusive process,[58] the fact that the PDF of the radial displacement Δr is very close to Gaussian provides another evidence of the diffusive process.[10,20,21] Both the skewness and the kurtosis are small. The particles used to measure the radial excursion are part of the plasma with both drag and scattering effects. The scattering effect dominates the radial diffusion (similar to passive particles) because of the constraints of the quasineutrality and adiabatic electrons.

The mean-squared displacements in Fig. 2 decreases with increasing energy after it peaks at an energy of $E=2T$, which is found to be consistent with the drift resonance condition of $\omega=\omega_d$, which is satisfied at $E=2.1T$ when averaging over the pitch, where $\omega_d=k_\theta v_d$ is the drift frequency, $v_d=(v^2+v_\parallel^2)/(2R\Omega)$ is the drift velocity, $\omega=k_\theta v_{ph}$ is the ITG diamagnetic frequency, Ω is the ion cyclotron frequency and $k_\theta=nq/r$ is the perpendicular wave number. The linear phase velocity v_{ph} is measured in the simulation and is roughly a constant[21] for the modes of $k_\theta\rho_i=[0,0.35]$, which have significant amplitudes in the nonlinear state.

A phase-space-resolved diffusivity can be defined as $D(E,\xi)=\Delta[\sigma^2(E,\xi;t)]/(2\Delta t)$ using the random walk model, since the radial excursion of the ions is diffusive. Here $\Delta[\sigma^2(E,\xi;t)]$ is the change in the standard deviation of the net radial excursions for each group of ions with energy E and pitch ξ during a time interval of Δt between $t_0=400L_T/v_i$ and $t_1=800L_T/v_i$ (when the turbulence is in a steady state). We restrict the simulation time span starting from t_0 when a steady state turbulence is active and ending at t_1 when the radial spread of the lower energy particles is still small enough to avoid strong boundary effect.

As a consistency check, the diffusivity of the thermal ions was calculated by averaging the phase-space diffusivity $D(E,\xi)$ over a Maxwellian distribution function with a temperature of T, $D_0=\int DF_M d^3\mathbf{v}$. It is found that this calculated diffusivity D_0 based on the random walk model is very close to an effective particle diffusivity D_i of thermal ions measured in the simulation, $D_0=1.1D_i$, where $D_i=2\chi_i/3$ and $\chi_i=3.1\chi_{\mathrm{GB}}$ are calculated from the self-consistent heat flux using $\chi_i=Q_i/(dT/dr)$. Here $Q_i=\int\frac{1}{2}v^2\delta v_r\delta f d^3\mathbf{v}$ is measured in the simulation, v is particle velocity, δf is the perturbed distribution function, and δv_r is the radial component of gyrophase-averaged $\mathbf{E}\times\mathbf{B}$ drift.

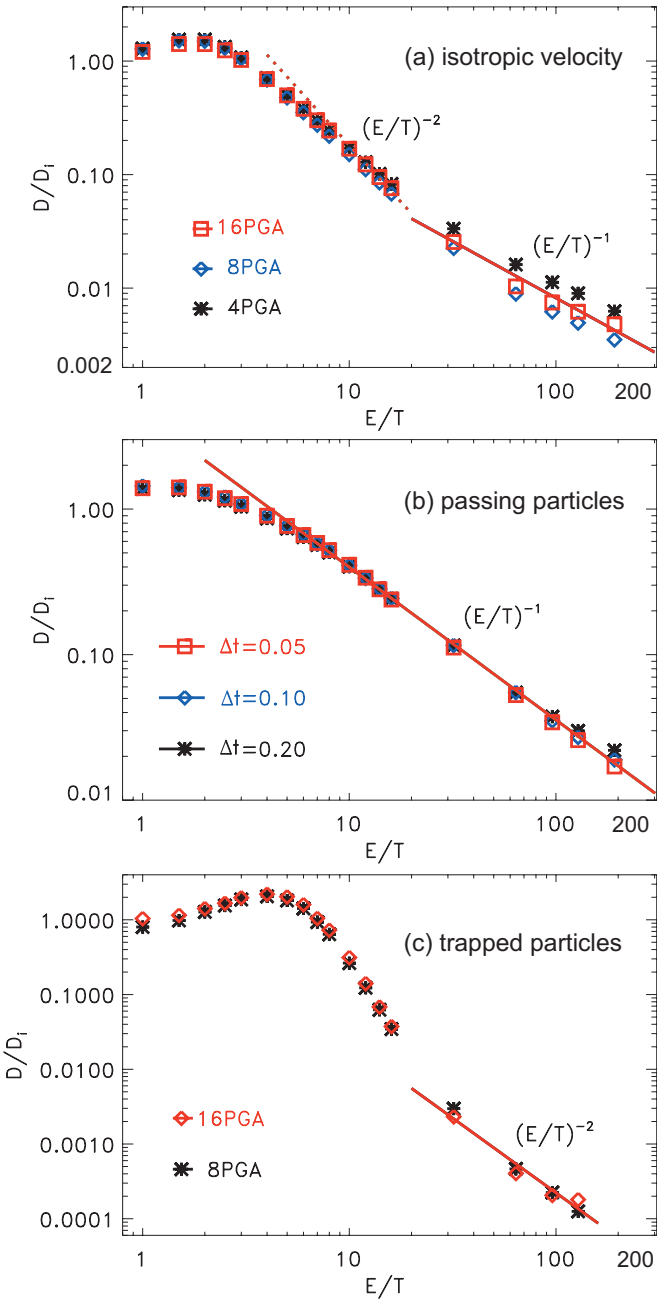

FIG. 4. (Color) Dependence of particle diffusivity D/D_i on particle energy E/T for (a) isotropic velocity distribution, (b) purely passing particles ($\mu=0$), and (c) deeply trapped particles ($v_\parallel\simeq 0$). The points are the simulation results using four-point (4PGA), four-point (8PGA, default), or 16-point (16PGA) gyroaveraging, or with time step from $0.2L_T/v_i$, $0.1L_T/v_i$ (default), down to $0.05L_T/v_i$. The straight lines are theoretical scaling laws $D\propto E^{-\alpha}$ with $\alpha=1$ and $\alpha=2$. Here, diffusivity of thermal ions is defined in terms of heat flux, $D_i=2\chi_i/3$.

B. Energy scaling of passing particle transport

The passing particles are loaded with a finite grid size in pitch angle space $\Delta\xi=1/80$, which numerically corresponds to a perpendicular velocity $v_\perp=0.16v$, and consequently, give rise to an effective gyroaveraging effect $J_0(0.16k_\perp\rho)$.[10] Here, ρ and v are the gyroradius and velocity of energetic particles, respectively, $k_\perp$ is the wave number in perpendicular direction. In order to eliminate this gyroaveraging effect for the purely passing particles, we initiated several runs without calculating the gyroaveraging effect of energetic particles, by turning off the FLR effect.[59] This enable us to investigate the transport of purely passing energetic particles, which gives a clear $(E/T)^{-1}$ scaling for energy $E/T)>5$ as displayed in Fig. 4(b).

The purely passing particles have large parallel velocity and thus high transit frequency $\omega_t=k_\parallel v_\parallel$. In order to truthfully capture the dynamics of the energetic passing particles, the parallel component of the Courant–Fiedrichs–Lewy condition, $v_\parallel\Delta t/(qR)<0.1$ has been enforced in simulations to ensure accuracy. Beyond this minimum requirement, numerical

convergence with respect to the time step has been completed by reducing the time step from $0.2L_T/v_i$, $0.1L_T/v_i$, down to $0.05L_T/v_i$. As shown in Fig. 4(b), the points with $\Delta t=0.2L_T/v_i$ exhibit relatively larger deviations from the other two groups when energy larger than $64T$. On the other hand, when the time step decreases from $\Delta t=0.1L_T/v_i$ to $\Delta t=0.05L_T/v_i$, particle diffusivity and other statistically significant quantities, such as fluctuation intensity, change very small. For the trapped particles discussed in Sec. III C with smaller parallel velocity and, correspondingly, longer bounce time, $\Delta t=0.1L_T/v_i$ is sufficient for these energetic-particle transport simulations and is set to the default time step.

The transport scaling for purely passing particles has been obtained by fitting the simulation points in Fig. 4(b) from the midrange through the high energy end with the power-law form, which is found to be a simple inverse proportionality, $D\propto(E/T)^{-1}$. The physical mechanics responsible for this scaling has been clarified using the quasilinear theory[10,30] of the diffusivity for passing particles. The drift orbit averaging gives a dependence of the diffusivity D on the energy through the Bessel function $J_0^2(k_\perp\rho_d)$. Here, $\rho_d\approx 2qv_\parallel/\Omega_i$ is the guiding center drift orbit size, $k_\perp$ is the wave number in the perpendicular direction. The orbit-averaging effects can be calculated by performing an average with the poloidal spectrum measured in the simulation. The orbit averaging is found to give a $(E/T)^{-1/2}$ dependence when $E>16T$. For purely passing particles, the resonance condition becomes $\omega_{\rm ITG}=k_\parallel v_\parallel$ locally along the field line, which gives rise to a $(E/T)^{-1/2}$ dependence of D. So we expect a diffusivity $D\propto(E/T)^{-1}$ for energetic passing particles, as confirmed in the GTC simulations. Here the orbit averaging requires that the turbulence eddy turn-over time is long enough to allow the energetic particles finish a complete parallel motion, i.e., $\omega_{\rm ITG}<k_\parallel v_\parallel$, which is satisfied by all the particles with energy higher than the critical value $E_{\rm cirt}/T\simeq 1.2$.

C. Energy scaling of trapped particle transport

To understand the transport scaling for trapped particles, we initialed several runs with the energetic particles loaded in a small rectangular region, $0.45a<r<0.55a$ and $-0.1<\theta<0.1$, in the real space, and $\xi\in[0,0.0276]$ or $\mu B/E\in[0.9992,1.0]$ in pitch angle or magnetic moment space, respectively. By this special initialization we are able to focus on the transport of deeply trapped energetic particles, which gives a clear $(E/T)^{-2}$ scaling when the simulation points in the high energy end are fitted by a power-law form as displayed in Fig. 4(c).

The transport simulation of deeply trapped particles relies on the accuracy of gyroaveraging in calculating the FLR effect.[59] Therefore, numerical convergence with respect to the number of points in the gyroaveraging has been carefully achieved by comparing the four-, eight- and 16-point gyroaveraging results. Generally, for fluctuations with $k_\theta\rho_\perp<2$, accuracy up to 4% can be achieved by using the four-point gyroaveraging method,[59] which is adequate for the ITG simulations with a single thermal species, where the maximum linear growth rate occurs around $k_\theta\rho_\perp=0.35$ with the current parameters. For deeply trapped particles in particular, the results from the four-point averaging show a large deviation from those from eight-point and 16-point for the high energy particles with $E/T>32$, while the diffusivity changes little when number of gyroaveraging points changes from 8 to 16, as evident in Fig. 4(c), as well as Fig. 4(a). This indicates the we need the eight-point gyroaveraging for $E/T>32$.

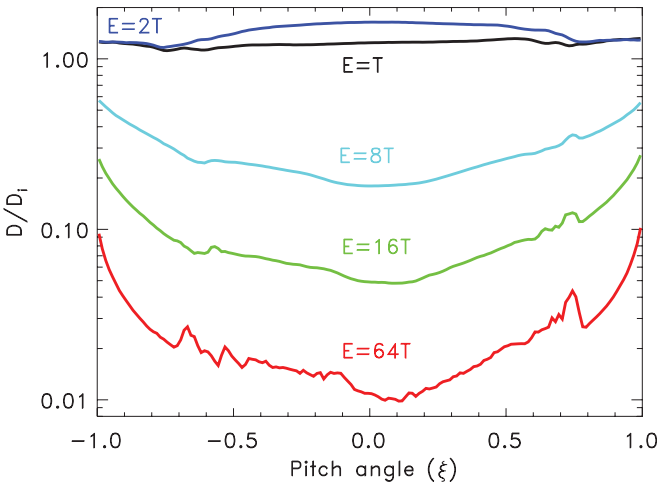

FIG. 5. (Color) Diffusivity D/D_i as a function of pitch angle $\xi=v_\parallel/v$ for particle energy of the following: T_e (black), $2T_e$ (blue), $16T_e$ (green), and $64T_e$ (red).

To understand the physical contributions to this energy scaling, we employed the quasilinear theory for deeply trapped particles. The gyroaveraging and the drift orbit averaging each gives rise to a dependence of D on $(E/T)^{-1/2}$ when energy $E/T>16$. Regarding the resonance condition, the frequencies $\omega_d,\omega_b\gg\omega$ when energy of fast particles is very high, then the resonance condition after bounce-averaging becomes $\omega_d=p\omega_b$ given $p>0$, or equivalently, $n\omega_{\rm pre}=p\omega_b$, where $\omega_{\rm pre}=qE/(mrR\Omega)$ is the precession frequency. This is the so-called drift-bounce resonance[30] accountable for the ripple loss process, which gives rise to another dependence of D on $(E/T)^{-1}$ when integrating over n since $\omega_{\rm pre}$ is proportional to E. Hence, for deeply trapped energetic particles, the diffusivity $D\propto(E/T)^{-2}$ taking into account both the orbit averaging and the decorrelation process. Here the orbit averaging is valid when particle energy is higher than $13T$ so that the bounce time is so short that a complete bounce motion is permitted during a turbulence decorrelation time.

D. Energy scaling of isotropic particle transport

The pitch-angle-averaged radial diffusivity of energetic particles as a function of the energy (E/T) is plotted in Fig. 4(a), where we use the default time step $\Delta t=0.1L_T/v_i$ based on the time step benchmark of passing particles discussed previously.

The diffusivity shown in Fig. 4(a) peaks at the resonant energy of $E/T=2$, remains significant for the low energy $(E/T<10)$ particles and decreases drastically for higher energy $(E/T>10)$ particles. This is a result of the averaging

effects of the large gyroradius and orbit width, and the fast decorrelation of the energetic particles with the waves for the high energy particles.[10]

The transport scaling of energetic particles is obtained by fitting the simulation points in the Fig. 4 using the simplest power-law form $D(E,\xi)=A(\xi)E^{\alpha}$ with A a constant. It can be found that in the midrange from $4T$ to $16T$, where trapped particles and passing particles are both important to the overall diffusivity, the index of the pitch-angle averaged diffusivity is close to $\alpha\approx-2$; in the high energy end, the diffusivity is close to a $(E/T)^{-1}$ scaling, which is the transport scaling of the purely passing particles, since the passing particles dominate over the trapped particles in the high energy limit, as shown in Figs. 4(b) and 4(c).

The pitch-angle dependence of the diffusivity is shown in Fig. 5. Compared with the transport level of passing particles, the transport of trapped particles is similar for thermal ions, is less but still in the same order for mildly energetic particles $(E/T<10)$, and negligible for the highly energetic particles $(E/T>10)$.

IV. SUMMARY

The energy scaling for energetic-particle transport by ITG microturbulence produced by background plasmas has been investigated through large-scale gyrokinetic particle simulations. GTC simulations show that, in high energy regime, transport scaling for passing particles is $D\propto(E/T)^{-1}$, due to the drift orbit averaging and decorrelation of parallel resonance. Transport scaling for trapped particles is $D\propto(E/T)^{-2}$, due to gyroaveraging, banana-orbit averaging and decorrelation of drift-bounce resonance.

Results from GTC simulations explained many features of the fast-ion $(E/T\lesssim10)$ transport in beam-heated DIII-D plasmas[15,16] using a simple model. GTC simulations verifies conventional concept that the energetic particle transport is reduced by gyroaveraging and drift orbit averaging and fast wave-particle decorrelation. Transport of α-particles $(E/T>10)$ are negligible, which is a good news for α-particle confinement in the burning plasmas. Transport of low energy α-particles $(E/T\lesssim10)$ is relatively strong, which may be good for ash removal.

ACKNOWLEDGMENTS

We would like to thank W. Heidbrink and Y. Nishimura for useful discussions. This work was supported by the U.S. Department of Energy (DOE) SciDAC GSEP and GPS-TTBP centers, and DOE and NSF grants at UC Irvine. L.C. also acknowledges support from National Basic Research Programs of China and National Special Research Program of China for ITER. Simulations used supercomputers at NERSC and ORNL.

[1] C. Z. Cheng, L. Chen, and M. S. Chance, Ann. Phys. **161**, 21 (1985).
[2] W. Horton, Rev. Mod. Phys. **71**, 735 (1999).
[3] A. B. Rechester and M. N. Rosenbluth, Phys. Rev. Lett. **40**, 38 (1978).
[4] W. W. Heidbrink and G. J. Sadler, Nucl. Fusion **34**, 535 (1994).
[5] See: http://www.iter.org.
[6] J. Giacalone and J. R. Jokipii, Astrophys. J. **520**, 204 (1999).
[7] R. White and H. Mynick, Phys. Fluids B **1**, 980 (1989).
[8] G. Manfredi and R. O. Dendy, Phys. Rev. Lett. **76**, 4360 (1996).
[9] S. J. Zweben, R. V. Budny, D. S. Darrow, S. S. Medley, R. Nazikian, B. C. Stratton, E. J. Synakowski, G. Taylor, and T. Grp, Nucl. Fusion **40**, 91 (2000).
[10] W. Zhang, Z. Lin, and L. Chen, Phys. Rev. Lett. **101**, 095001 (2008).
[11] C. Angioni and A. Peeters, Phys. Plasmas **15**, 052307 (2008).
[12] C. Angioni, A. G. Peeters, G. V. Pereverzev, A. Bottino, J. Candy, R. Dux, E. Fable, T. Hein, and R. E. Waltz, Nucl. Fusion **49**, 055013 (2009).
[13] S. Gunter, G. Conway, S. DaGraca, H. U. Fahrbach, C. Forest, M. G. Munoz, T. Hauff, J. Hobirk, V. Igochine, F. Jenko, K. Lackner, P. Lauber, P. McCarthy, M. Maraschek, P. Martin, E. Poli, K. Sassenberg, E. Strumberger, G. Tardini, E. Wolfrum, H. Zohm, and ASDEX Upgrade Team, Nucl. Fusion **47**, 920 (2007).
[14] T. Suzuki, S. Ide, T. Oikawa, T. Fujita, M. Ishikawa, M. Seki, G. Matsunaga, T. Hatae, O. Naito, K. Hamamatsu, M. Sueoka, H. Hosoyama, M. Nakazato, and JT-60 Team, Nucl. Fusion **48**, 045002 (2008).
[15] W. W. Heidbrink, J. M. Park, M. Murakami, C. C. Petty, C. Holcomb, and M. A. Van Zeeland, Phys. Rev. Lett. **103**, 175001 (2009).
[16] W. W. Heidbrink, M. Murakami, J. M. Park, C. C. Petty, M. A. Van Zeeland, J. H. Yu, and G. R. McKee, Plasma Phys. Controlled Fusion **51**, 125001 (2009).
[17] M. Vlad and F. Spineanu, Plasma Phys. Controlled Fusion **47**, 281 (2005).
[18] C. Estrada-Mila, J. Candy, and R. E. Waltz, Phys. Plasmas **13**, 112303 (2006).
[19] Z. Lin, T. Hahm, W. Lee, W. Tang, and R. White, Science **281**, 1835 (1998).
[20] Z. Lin, S. Ethier, T. Hahm, and W. Tang, Phys. Rev. Lett. **88**, 195004 (2002).
[21] Z. Lin and T. S. Hahm, Phys. Plasmas **11**, 1099 (2004).
[22] H. Goldstein, *Classical Mechanics*, 2nd ed. (Addison-Wesley, Reading, MA, 1980).
[23] E. Ott, *Chaos in Dynamical Systems*, 2nd ed. (Cambridge University Press, New York, 2002).
[24] A. Lichtenberg and M. Lieberman, *Regular and Chaotic Dynamics*, 2nd ed. (Spinger-Verlag, Berlin, 1992).
[25] H. E. Mynick, Phys. Rev. Lett. **43**, 1019 (1979).
[26] H. E. Mynick, Nucl. Fusion **26**, 491 (1986).
[27] H. E. Mynick and R. E. Duvall, Phys. Fluids B **1**, 750 (1989).
[28] J. R. Myra and P. J. Catto, Phys. Fluids B **4**, 176 (1992).
[29] J. R. Myra, P. J. Catto, H. E. Mynick, and R. E. Duvall, Phys. Fluids B **5**, 1160 (1993).
[30] L. Chen, J. Geophys. Res., [Space Phys.] **104**, 2421, doi:10.1029/1998JA900051 (1999).
[31] T. S. Hahm and W. M. Tang, Phys. Plasmas **3**, 242 (1996).
[32] B. H. Fong and T. S. Hahm, Phys. Plasmas **6**, 188 (1999).
[33] F. Zonca, P. Buratti, A. Cardinali, L. Chen, J. Q. Dong, Y. X. Long, A. V. Milovanov, F. Romanelli, P. Smeulders, L. Wang, Z.-T. Wang, C. Castaldo, R. Cesario, E. Giovannozzi, M. Marinucci, and V. Pericoli Ridolfini, Nucl. Fusion **47**, 1588 (2007).
[34] L. Wang and T. S. Hahm, Phys. Plasmas **16**, 12 (2009).
[35] P. J. Catto, W. M. Tang, and D. E. Baldwin, Plasma Phys. Controlled Fusion **23**, 639 (1981).
[36] E. A. Frieman and L. Chen, Phys. Fluids **25**, 502 (1982).
[37] T. S. Hahm, Phys. Fluids **31**, 2670 (1988).
[38] A. J. Brizard and T. S. Hahm, Rev. Mod. Phys. **79**, 421 (2007).
[39] J. R. Cary and A. J. Brizard, Rev. Mod. Phys. **81**, 693 (2009).
[40] T. Hauff, M. J. Pueschel, T. Dannert, and F. Jenko, Phys. Rev. Lett. **102**, 075004 (2009).
[41] T. Hauff and F. Jenko, Phys. Plasmas **15**, 112307 (2008).
[42] T. Hauff and F. Jenko, Phys. Plasmas **16**, 102306 (2009).
[43] M. Albergante, J. P. Graves, A. Fasoli, F. Jenko, and T. Dannert, Phys. Plasmas **16**, 112301 (2009).
[44] C. Greenfield, J. DeBoo, T. Osborne, F. Perkins, M. Rosenbluth, and D. Boucher, Nucl. Fusion **37**, 1215 (1997).
[45] Z. Lin, T. S. Hahm, W. W. Lee, W. M. Tang, and P. H. Diamond, Phys. Rev. Lett. **83**, 3645 (1999).
[46] P. H. Diamond, M. N. Rosenbluth, F. L. Hinton, M. Malkov, J. Fleischer, and A. Smolyakov, Proceedings of the 17th IAEA Fusion Energy Conference, Yokohama, Japan, 1998.
[47] L. Chen, Z. Lin, and R. White, Phys. Plasmas **7**, 3129 (2000).
[48] T. S. Hahm, M. A. Beer, Z. Lin, G. W. Hammett, W. W. Lee, and W. M. Tang, Phys. Plasmas **6**, 922 (1999).
[49] G. Rewoldt, Z. Lin, and Y. Idomura, Comput. Phys. Commun. **177**, 775 (2007).

[50]I. Holod and Z. Lin, Phys. Plasmas **14**, 032306 (2007).
[51]C. S. Chang, S. Ku, P. H. Diamond, Z. Lin, S. Parker, T. S. Hahm, and N. Samatova, Phys. Plasmas **16**, 056108 (2009).
[52]S. Ku, C. Chang, and P. Diamond, Nucl. Fusion **49**, 115021 (2009).
[53]V. K. Decyk, C. D. Norton, and B. K. Szymanski, Sci. Prog. **6**, 363 (1997).
[54]V. K. Decyk and H. J. Gardner, Comput. Phys. Commun. **178**, 611 (2008).
[55]Z. Lin, I. Holod, L. Chen, P. H. Diamond, T. S. Hahm, and S. Ethier, Phys. Rev. Lett. **99**, 265003 (2007).
[56]I. Holod and Z. Lin, Phys. Plasmas **15**, 092302 (2008).
[57]Y. Xiao and Z. Lin, Phys. Rev. Lett. **103**, 085004 (2009).
[58]R. Sánchez, D. E. Newman, J. N. Leboeuf, V. K. Decyk, and B. A. Carreras, Phys. Rev. Lett. **101**, 205002 (2008).
[59]W. W. Lee, J. Comput. Phys. **72**, 243 (1987).